ACS APPLIED MATERIALS & INTERFACES

Research Article

Cite This: ACS Appl. Mater. Interfaces 2018, 10, 11143−11151

www.acsami.org

Band Engineering of Carbon Nitride Monolayers by N-Type, P-Type, and Isoelectronic Doping for Photocatalytic Applications

Meysam Makaremi,[†] Sean Grixti,[†] Keith T. Butler,[‡] Geoffrey A. Ozin,[§] and Chandra Veer Singh*[,†,∥]

[†]Department of Materials Science and Engineering, University of Toronto, 184 College Street, Suite 140, Toronto ON M5S 3E4, Canada

[‡]Centre for Sustainable Chemical Technologies and Department of Chemistry, University of Bath, Bath BA2 7AY, United Kingdom

[§]Department of Chemistry, Solar Fuels Research Cluster, University of Toronto, 80 St. George Street, Toronto ON M5S 3H6, Canada

[∥]Department of Mechanical and Industrial Engineering, University of Toronto, 5 King's College Road, Toronto ON M5S 3G8, Canada

Supporting Information

ABSTRACT: Since hydrogen fuel involves the highest energy density among all fuels, production of this gas through the solar water splitting approach has been suggested as a green remedy for greenhouse environmental issues due to extensive consumption of fossil fuels. Low-dimensional materials possessing a large surface-to-volume ratio can be a promising candidate to be used for the photocatalytic approach. Here, we used extensive first-principles calculations to investigate the application of newly fabricated members of two-dimensional carbon nitrides including *tg*-C_3N_4, *hg*-C_3N_4, C_2N, and C_3N for water splitting. Band engineering via N-type, P-type, and isoelectronic doping agents such as B, N, P, Si, and Ge was demonstrated for tuning the electronic structure, optimizing solar absorption and band alignment for photocatalysis. Pristine *tg*-C_3N_4, *hg*-C_3N_4, and C_2N crystals involve bandgaps of 3.190, 2.772, and 2.465 eV, respectively, which are not proper for water splitting. Among the dopants, Si and Ge dopants can narrow the band gap of carbon nitrides about 0.5−1.0 eV and also increase their optical absorption in the visible spectrum. This study presents the potential for doping with isoelectronic elements to greatly improve the photocatalytic characteristics of carbon nitride nanostructures.

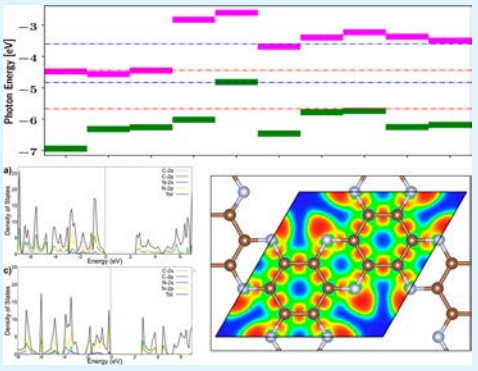

KEYWORDS: *carbon nitride, water splitting, density functional theory, band structure, band edge position, solar absorption spectrum*

1. INTRODUCTION

A rapidly growing human population and extensive fossil fuel energy consumption leading to environmental issues have motivated scientists to device new techniques to extract and store reliable green energy from renewable natural sources such as wind, water, biomass, and sunlight. Specifically sustainable energy systems and applications involving the production of hydrogen fuel from water have been the research focus during the recent years.[1−4] For the first time in 1972, water was split into H_2 and O_2 through a solar electrochemical approach, and the breaking of the water molecule emerged as a clean and reliable remedy for future energy issues.[5−7] In solar water splitting, H_2, which is a clean fuel and contains the highest energy density (∼142 MJ kg^{-1}) among fuels, is the final product.[8−10]

Progress in the green energy industry can greatly benefit from contemporary advances in the development of low-dimensional nanostructures such as nanoparticles, nanotubes, and two-dimensional (2D) materials, which demonstrate fascinating properties for optoelectronic, catalytic, and energy storage/conversion applications stemming from their large surface-to-volume ratios.[11,12] There had been a great enthusiasm to extract 2D graphene from the bulk structure of graphite for decades until finally Novoselov et al. mechanically exfoliated graphite and isolated the carbon monolayer in 2004.[13] Physical properties of graphene, including fascinating thermal, optical, mechanical, and electronic characteristics, generated a flurry of research activity to uncover other 2D materials.[14−16]

In the past decade, a broad spectrum of 2D materials has been predicted, fabricated, and characterized.[17−19] These materials may involve only single elements such as graphene, germanene, and stanene,[20] or they might contain binary/multiplinary structures such as boron nitride (BN),[21,22] transition metal oxides (TMOs),[23,24] transition metal dichalcogenides (TMDs),[25−28] and metal nitrides/carbides/carbonitrides (MXenes).[29,30] Two approaches including top-down and bottom-up techniques are employed to fabricate the mono-

Received: January 30, 2018
Accepted: March 19, 2018
Published: March 19, 2018

DOI: 10.1021/acsami.8b01729
ACS Appl. Mater. Interfaces 2018, 10, 11143−11151

layers.[31−33] The former generates the nanosheet from the bulk structure by the means of physical exfoliation, while the latter synthesizes the monolayer by linking the unit blocks via chemical reaction.[34] Recently, carbon nitride nanosheets (2D-CN) including C_3N_4,[35,36] C_2N,[37] and C_3N[38] have been synthesized through bottom-up procedures.

2D-CN nanostructures show outstanding optical, thermal, mechanical, and electronic properties due to their strong atomic networks composed of C and N atoms, which have comparable atomic sizes and contain four and five valence electrons, respectively, forming consistent covalent configurations.[39−41] C_3N_4 can exist in different configurations including the cubic phase, semicubic phase, α-phase, β-phase, and graphitic (g) phase in two forms (*hg*-C_3N_4 and *tg*-C_3N_4), among which g-phases are known to be the most stable phases with the nonmetallic nature including energy gaps of 2.7 and 3.1 eV.[42−44] Nitrogenated holey graphene is another carbon nitride nanosheet with a stoichiometric formula of C_2N, which contains an evenly distributed network of N and hole sites, which makes it an excellent candidate as a nanofilter for shape and size selective adsorption of different ions, atoms, and molecules.[37,45] Lately, 2D polyaniline with one N and three C atoms per unit cell (C_3N) have been fabricated, and it is found to have amazing optical, thermal, mechanical, electronic, and magnetic properties.[46−48] Additional degrees of freedom are provided by the ability to dope these materials, facilitating the engineering of band structures to tailor the system for a given application. This wide compositional and structural possibilities, however, is daunting to explore exhaustively by synthesis and characterization.

Computational modeling allows for the understanding and development of general design principles. While there has been limited theoretical studies, an in depth survey of trends across the range of different carbon nitride nanosheets, with various doping regimes, is still lacking.[49−52] The recent successful fabrication of different carbon nitride nanosheets including *hg*-C_3N_4, *tg*-C_3N_4, C_2N, and C_3N with fascinating semiconducting behaviors prompted us to consider the possible application of these materials for solar water splitting by tuning the bandgap.[35−38] We carried out extensive density functional theory (DFT) simulations to tune the bandgap through N-type, P-type, and isoelectronic doping with different elements consisting of B, N, P, Si, and Ge dopants. We used different electronic structure calculations including structural relaxation, adsorption energy, electronic density of states, band energy alignment, and absorbance spectrum analyses.

2. COMPUTATIONAL DETAILS

Perdew−Burke−Ernzerhof (PBE)[53] and Heyd−Scuseria−Ernzerhof (HSE06)[54] density functional theory (DFT) techniques implemented in the Vienna Ab initio Simulation Package (VASP)[55] were employed via generalized gradient approximation (GGA) and projector augmented-wave (PAW) potentials.[56] A kinetic energy cutoff of 500 eV, electronic self-consistency of 1×10^{-6} eV, and ionic relaxation convergence of 1×10^{-3} eV/Å were applied. Also, a Grimme dispersion correction technique, DFT-D2,[57] was considered to modify van der Waals energy calculations. Monkhorst−Pack grids of 15 × 15 × 1 and 6 × 6 × 1 were used for PBE and HSE06 calculations, respectively, and the tetrahedron scheme with Blöchl corrections was employed to integrate the Brillouin zone.

The optical response of 2D structures was evaluated by complex dielectric function calculations.[58] The function, which is composed of the real (ϵ^1) and imaginary (ϵ^2) parts, can be determined by

$$\epsilon^1(\omega) = 1 + \frac{2}{\pi} p \int \frac{\epsilon^2(\omega')\omega'}{\omega'^2 - \omega^2} d\omega' \quad (1)$$

$$\epsilon^2(\omega) = \frac{4\pi^2 e^2}{m^2\omega^2} \sum_{c,v} \int \frac{|P_{c,v}(k)|^2}{\nabla\omega_{c,v}(k)} dC_k \quad (2)$$

here, C_k and P are the surface-energy constant and the principle part of the ϵ^1 integral, respectively. $P_{c,v}$ and $\omega_{c,v}$ are the dipole and energy difference matrix element between conduction (c) and valence (v) states, respectively. The absorption coefficient $\alpha(\omega)$ can be described as

$$\alpha(\omega) = \sqrt{2\omega}\{\sqrt{\epsilon^1(\omega)^2 + \epsilon^2(\omega)^2} - \epsilon^1(\omega)\}^{1/2} \quad (3)$$

The unit cells of each carbon nitride nanosheet used are described as follows: the unit cell of C_2N has 12 carbon atoms and 6 nitrogen atoms, and it can be characterized as 2 interconnected benzene rings via a pyrazine ring. The C_3N unit cell has 6 carbon atoms and 2 nitrogen atoms and has a honeycomb structure, similar to graphene. The *tg*-C_3N_4 unit cell has 3 carbon atoms and 4 nitrogen atoms and is characterized as interconnected triazine molecules bridged by nitrogen atoms. The *hg*-C_3N_4 unit cell has 6 carbon atoms and 8 nitrogen atoms and is characterized as an array of interconnected heptazine molecules bridged by nitrogen atoms.

3. RESULTS AND DISCUSSION

The relaxed atomic structures of pristine carbon nitride nanosheets including C_2N, C_3N, *tg*-C_3N_4, and *hg*-C_3N_4 can be seen in Figure 1. The lattice parameters of the PBE relaxed C_2N unit cell were determined to be a = 8.263 Å and γ = 60°, which is in good agreement with previous simulations and experimental data.[37,52,59] The lattice parameters of the PBE relaxed C_3N unit cell were determined to be a = 4.861 Å and γ = 120°, which is also in good agreement with previous results.[38,60] The lattice parameters of the PBE relaxed *tg*-C_3N_4 unit cell were determined to be a = 4.783 Å and γ = 120°, which is in good agreement with previous results.[61] The lattice

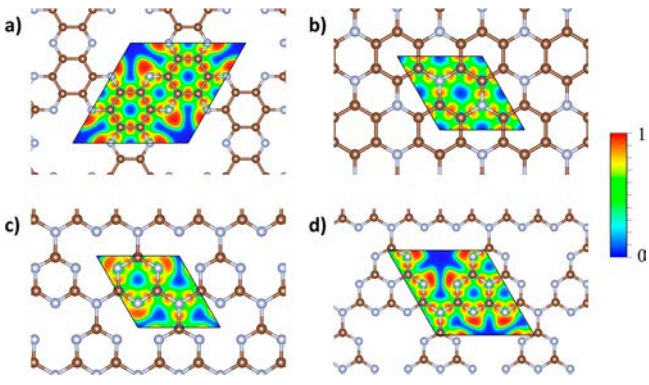

Figure 1. Structures of carbon nitrides: (a) C_2N, (b) C_3N, (c) *tg*-C_3N_4, and (d) *hg*-C_3N_4. The contours illustrate the electron localization function (ELF), which has a value between 0 and 1, where 1 corresponds to the perfect localization. Tthe brown atoms represent carbon, and the blue atoms represent nitrogen.

DOI: 10.1021/acsami.8b01729
ACS Appl. Mater. Interfaces 2018, 10, 11143−11151

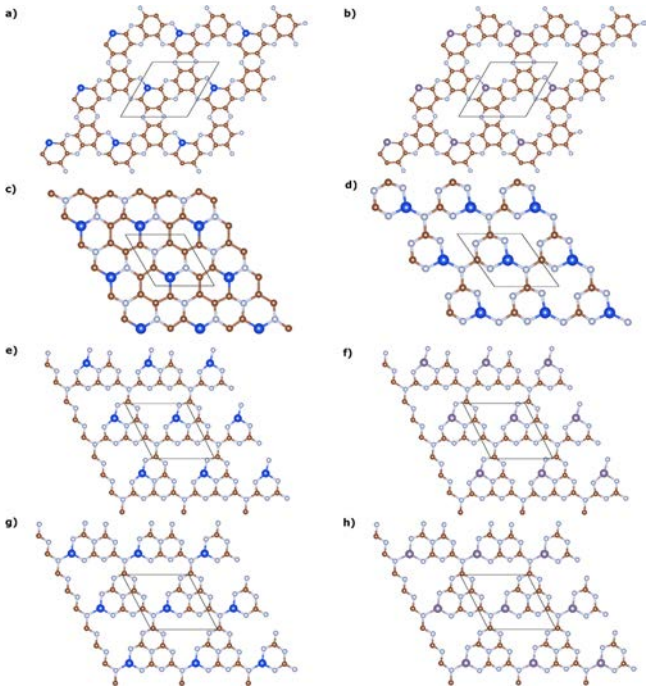

Figure 2. Structures of the doped semiconducting carbon nitrides: (a) $C_{2-x}Si_xN$, (b) $C_{2-x}Ge_xN$, (c) $C_{3-x}Si_xN$, (d) *tg*-$C_{3-x}Si_xN_4$, (e) *hg*-$C_{3-x}Si_xN_4$ *corner site*, (f) *hg*-$C_{3-x}Ge_xN_4$ *corner site*, (g) *hg*-$C_{3-x}Si_xN_4$ *bay site*, and (h) *hg*-$C_{3-x}Ge_xN_4$ *bay site*. Brown atoms represent carbon, light blue atoms represent nitrogen, royal blue atoms represent silicon, and purple represents germanium.

parameters of the PBE relaxed *hg*-C_3N_4 unit cell were determined to be a = 7.133 Å and γ = 120°, which is also in good agreement with previous results.[35,61]

Furthermore, the electron localization function (ELF)[62] of different CN structures is depicted in Figure 1. The normalized ELF contour involves a spectrum ranging from values of 0 to 1, in which 0 (blue) and 1 (red) present a lack and abundance of electron localization, respectively. If the ELF contour is located at the center of a bond, it shows covalent bonding, while if the pronounced localization contour is located on one side of the bond (on one of the atoms), it illustrates ionic bonding.[63] Each CN structure involves two different bonds including C−C and C−N bonds. The electron localization at the middle of both bonds for each lattice illustrates covalent bonding between C−C and C−N atoms; moreover, CN crystals contain two kinds of N atoms with respect to the number of bonded atoms, including two or three C atoms. There is a charge localization on the former type of N atoms, showing that these bonds have stronger ionic properties and a weaker covalent nature compared to the latter type.

Doping each carbon nitride on the carbon site was attempted with B, N, P, Si, and Ge as dopants. The relaxed structure of the successfully doped systems can be seen in Figures 2 and S1, and structural characteristics of the doped carbon nitride materials can be seen in Tables 1, 2, S1, and S2. We note that the doping of Ge into the carbon site of C_3N and *tg*-C_3N_4 causes structural collapse for C_3N and the formation of a new phase completely different from the initial *tg*-C_3N_4 structure, respectively, and so their properties are not reported. A trend of increasing structural deformation with increasing dopant atomic size is noted, as expected, with distortions in atomic structure and unit cell lattice parameters being present. From the successfully doped systems, electronic structure calculations were performed to determine their applicability for photocatalytic water splitting applications.

In Tables 1−3, the band gap of each pristine and doped carbon nitride system is reported. The band gaps obtained from using the PBE functional for C_2N, C_3N, *hg*-C_3N_4 and *tg*-C_3N_4 were 1.660, 0.386, 1.197, and 1.574 eV, respectively. Since the PBE functional is known to underestimate band gaps, hybrid functional calculations with the HSE-06 functional were performed on each of the relaxed structures. The band gaps obtained from using the HSE-06 functional for C_2N, C_3N, *hg*-C_3N_4, and *tg*-C_3N_4 were 2.465, 1.049, 2.772, and 3.190 eV, respectively. The band gaps obtained from the HSE-06 functional are more than double the value of the band gaps obtained from the PBE functional. The band gaps obtained from the HSE-06 functional match literature values very well, as seen in Table 3, with previous reports of 2.47, 1.042, 2.72, and 3.1 eV for C_2N, C_3N, *hg*-C_3N_4, and *tg*-C_3N_4, respectively.[35,52,60,64]

In Figure 3, the total density of states and projected orbital density of states of each pristine system is shown. It is noted that there is significant hybridization between the carbon 2p states and the nitrogen 2p states in all systems. The C_p−N_p hybridization is the main bonding source in all pristine systems,

Table 1. Structural and Electronic Characteristics of Pristine and Doped C_2N and C_3N

C_2N lattice parameter	pristine	B	N	P	Si	Ge
a (Å)	8.326	8.544	8.325	8.703	8.841	8.965
b (Å)	8.326	8.357	8.302	8.415	8.418	8.433
γ (deg)	60	59.73	59.32	59.88	59.83	59.77
band gap (eV)						
PBE	1.660	metallic	metallic	metallic	1.158	1.103
HSE-06	2.465	metallic	metallic	metallic	1.754	1.810
C_3N lattice parameter	pristine	B	N	P	Si	
a (Å)	4.861	4.927	4.831	5.139	5.193	
b (Å)	4.861	4.948	4.831	5.156	5.232	
γ (deg)	120.00	120.00	120.00	120.11	120.25	
band gap (eV)						
PBE	0.386	metallic	metallic	metallic	metallic	
HSE-06	1.049	metallic	metallic	metallic	0.331	

DOI: 10.1021/acsami.8b01729
ACS Appl. Mater. Interfaces 2018, 10, 11143−11151

Table 2. Structural and Electronic Characteristics of Pristine and Doped *tg*-C_3N_4 and *hg*-C_3N_4

tg-C_3N_4 lattice parameter	pristine	B	N	P	Si	
a (Å)	4.783	4.961	4.732	5.203	5.338	
b (Å)	4.783	4.961	4.732	5.203	5.342	
γ (deg)	120	124.76	119.08	123.91	125.25	
band gap (eV)						
PBE	1.574	metallic	metallic	metallic	0.890	
HSE-06	3.190	metallic	metallic	metallic	2.209	
hg-C_3N_4 *corner site* lattice parameter	pristine	B	N	P	Si	Ge
a (Å)	7.134	7.094	7.127	7.250	7.288	7.400
b (Å)	7.133	7.096	7.126	7.251	7.290	7.398
γ (deg)	120.00	118.12	120.44	117.71	116.80	116.78
band gap (eV)						
PBE	1.197	metallic	metallic	metallic	0.913	1.070
HSE-06	2.772	metallic	metallic	metallic	2.385	2.508
bay site lattice parameter	pristine	B	N	P	Si	Ge
a (Å)	7.134	7.252	7.088	7.509	7.626	7.803
b (Å)	7.133	7.057	7.160	7.123	7.108	7.101
γ (deg)	120.00	119.12	120.35	118.30	117.69	117.33
band gap (eV)						
PBE	1.197	metallic	metallic	metallic	1.389	1.248
HSE-06	2.772	metallic	metallic	metallic	2.886	2.691

Table 3. Band Gaps of the Pristine Carbon Nitride Nanosheets

band gap (eV)	C_2N	C_3N	*tg*-C_3N_4	*hg*-C_3N_4
current work (HSE-06)	2.465	1.049	3.190	2.772
literature	2.47[48]	1.042[56]	3.1[59]	2.72[33]

originating from the combination of sp^2-sp^2 σ-bonding and p–p π-bonding. Significant hybridization between the carbon p-states, nitrogen p-states, and the dopant p-states is observed in all doped systems as well. When doped with aliovalent dopants, such as B, N, and P, all carbon nitride nanosheets become metallic. This is due to the significant p- and n-doping from the doping species. B p-dopes each system significantly, pushing the Fermi level into the valence band, making each system metallic, as seen in Figure S2. On the other hand, N and P both n-dope each system significantly, pushing the Fermi level into

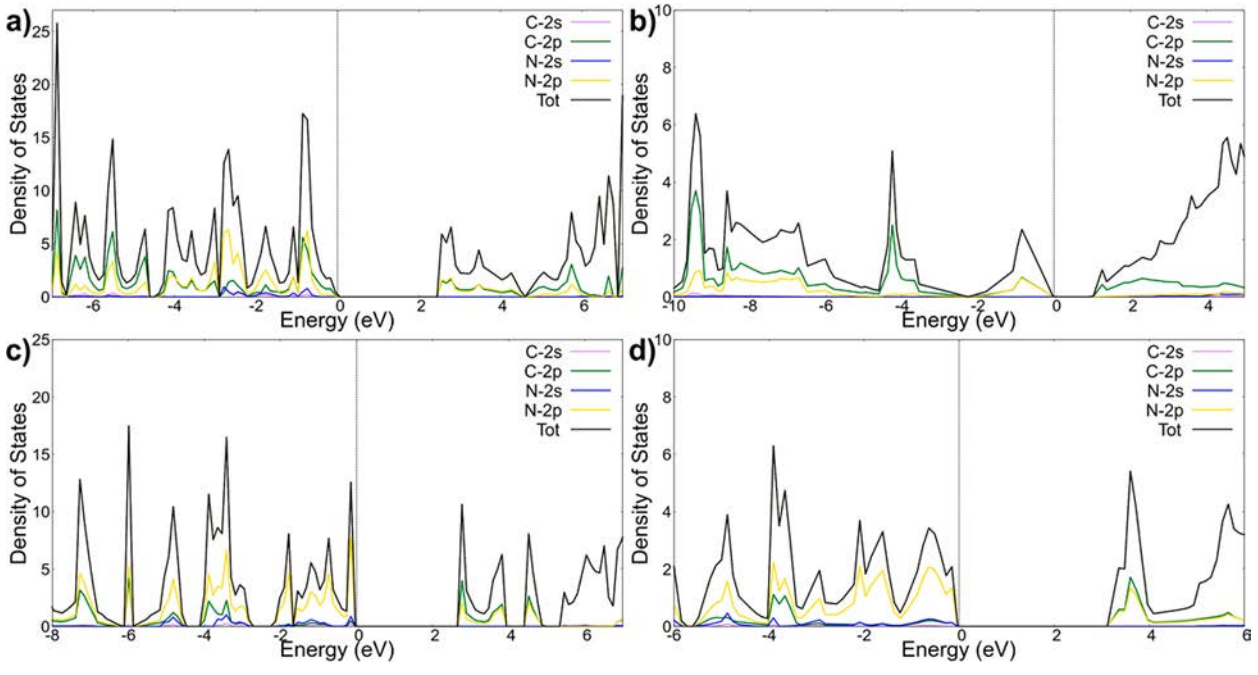

Figure 3. Projected density of states (PDOS) of the pristine carbon nitrides: (a) C_2N, (b) C_3N, (c) *hg*-C_3N_4, and (d) *tg*-C_3N_4.

DOI: 10.1021/acsami.8b01729
ACS Appl. Mater. Interfaces 2018, 10, 11143–11151

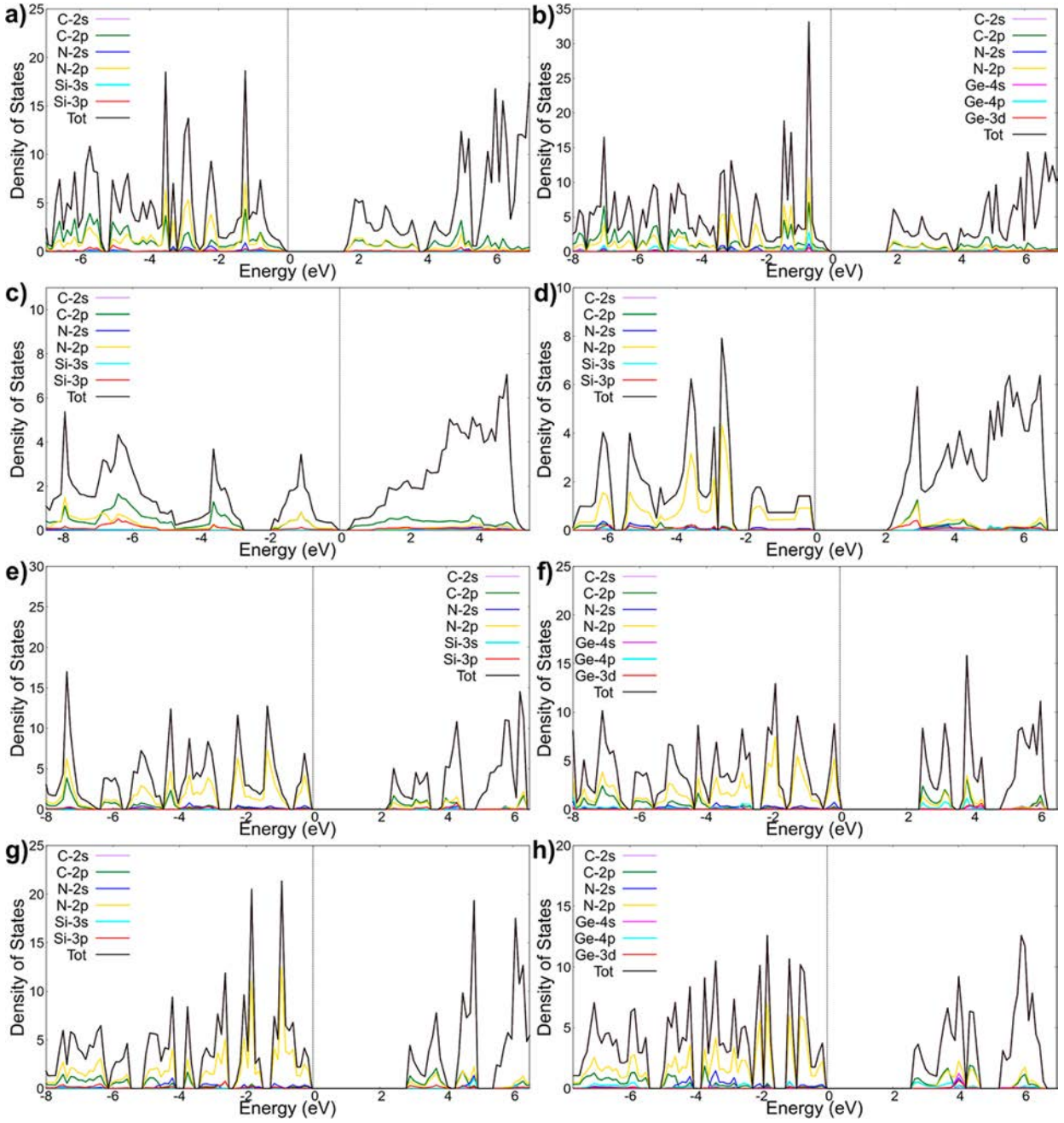

Figure 4. Projected density of states (PDOS) of the semiconducting doped carbon nitrides: (a) $C_{2-x}Si_xN$, (b) $C_{2-x}Ge_xN$, (c) $C_{3-x}Si_xN$, (d) *tg*-$C_{3-x}Si_xN4$, (e) *hg*-$C_{3-x}Si_xN_4$ in the *corner site*, (f) *hg*-$C_{3-x}Ge_xN_4$ in the *corner site*, (g) *hg*-$C_{3-x}Si_xN_4$ in the *bay site*, (h) *hg*-$C_{3-x}Ge_xN_4$ in the *bay site*.

the conduction band, making each system metallic, as seen in Figure S2.

When doped with isoelectronic dopants, the semiconducting character of each system is conserved; therefore band gap engineering is possible. When C_2N is doped with Si and Ge, the band gap narrows to 1.754 and 1.810 eV, respectively, from the 2.465 eV band gap of the pristine system. When C_3N is doped with Si, the band gap narrows from 1.042 to 0.331 eV. When *tg*-C_3N_4 is doped with Si, the band gap narrows to 2.209 from 3.190 eV. Band gap narrowing is also observed when doping *hg*-C_3N_4 in the corner site with Si and Ge and in the bay site with Ge, with the band gap narrowing from 2.772 to 2.385, 2.508, and 2.691 eV, respectively. This band gap narrowing is consistent with previous investigations into isoelectronic doping of graphene materials.[52,65]

The band gap narrowing that occurs with the isoelectronic dopants can be explained by a decrease bond strength and hybridization due to smaller orbital overlap. The larger dopant atom increases the bond distance and increases the ionicity of the bonding character, and therefore, decreases the orbital interaction with the smaller nitrogen and carbon atoms.[66] Since the valence band maximum (VBM) has a bonding character and the conduction band minimum (CBM) has an antibonding character, the decreased hybridization results in an effective upward shift of the VBM and downward shift of the CBM. However, it is noted that contrary to group IV band gap trends, Si provides greater band narrowing compared to Ge.[67−69] This

DOI: 10.1021/acsami.8b01729
ACS Appl. Mater. Interfaces 2018, 10, 11143−11151

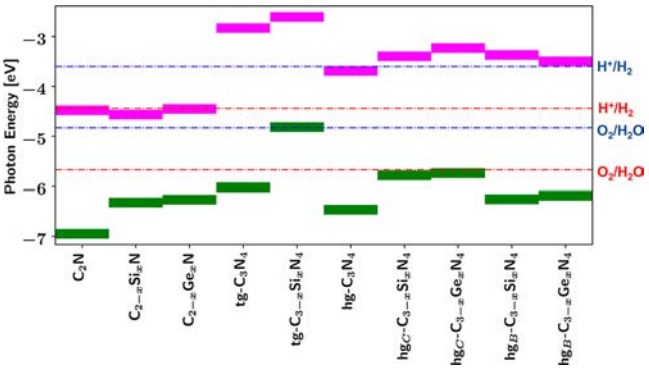

Figure 5. Valence (green) and conduction (magenta) band edge positions of pristine and doped carbon nitrides. The energies of the water splitting half reactions at pH 0 (red) and pH 14 (blue) are provided by the dashed lines. A conduction band above H^+/H_2 can drive this half reaction; a valence band below O_2/H_2O can drive this half reaction.

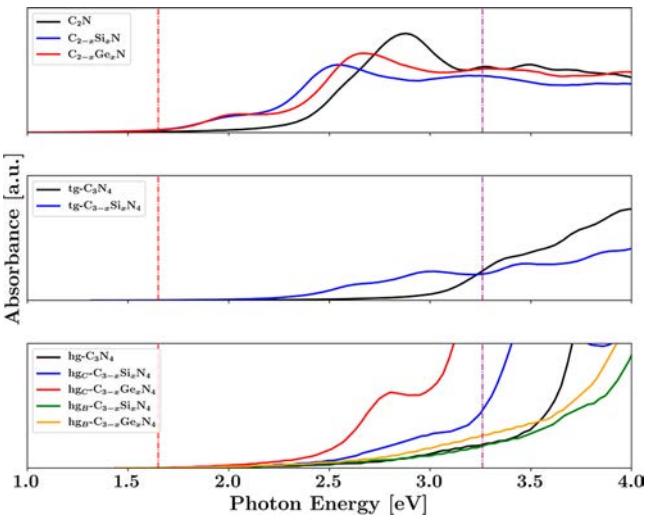

Figure 6. Absorption energy spectrum with respect to photon energy for pristine and doped C_2N, tg-C_3N_4, and hg-C_3N_4 structures. The spectra were calculated by using a PBE functional corrected by a rigid energy shift considered from HSE06 calculations. Dashed red and purple lines indicate the visible electromagnetic spectrum.

can be explained by the added bonding interaction from the 3d orbital of Ge hybridizing with the sp^2 orbitals of the neighboring atoms, as observed from the projected density of states in Figure 4.

Band widening occurs when Si is doped into the bay site of *hg*-C_3N_4, increasing the band gap from 2.772 to 2.886 eV. This deviation from the trend can be explained by the fact the bond distance does not significantly increase from pristine upon the addition of Si, and greater orbital overlap of the Si 3p orbitals with the neighboring 2p states is observed. This effect is not seen when Ge is doped into the bay site of *hg*-C_3N_4, even though the bond distance of does not increase significantly from pristine. Band widening does not occur when Ge is doped into the bay site, as the ionicity of the bonding character is greater, compared to Si, as observed by a lower Ge-4p density of states in Figure 4h.

The splitting of water involves two redox half reactions

$$\text{reduction: } 2H^+(aq) + 2e^- \rightarrow H_2(g) \quad (4)$$

$$\text{oxidation: } 2H_2O(l) \rightarrow O_2(g) + 4H^+(aq) + 4e^- \quad (5)$$

At pH = 0, the reduction potential of H^+/H_2 and the oxidation potential of O_2/H_2O are −4.44 and −5.67 eV, respectively; therefore, the minimal theoretical energy gap for a material to be applied to the solar water splitting process needs to be 1.23 eV.[70−72] As a consequence, among all of the 2D carbon nitride structures studied in this work, pristine C_2N, *tg*-C_3N_4, and *hg*-C_3N_4 crystals and their counterparts doped with Si and Ge warrant further investigation for photocatalytic applications.

The configuration of band edges is a key factor determining the applicability of a semiconductor for photocatalysis.[9] To be applied to solar water splitting, a material must possess a VBM less negative than the H^+/H_2 reduction potential and a CBM energy level more negative than the O_2/H_2O oxidation potential. Semiconducting 2D carbon nitride crystals including pristine and doped C_2N, *tg*-C_3N_4, and *hg*-C_3N_4 structures are illustrated in Figure 5 and compared with the reduction H^+/H_2 and oxidation O_2/H_2O energy levels of water splitting at two acidic (pH of 0) and basic (pH of 14) conditions.

Assessing the applicability of material for catalytic processes requires us to place the energies of active carriers in the material in relation to the redox energies of the reactions desired.[73] We use the alignment of the valence band maximum (for holes) and the conduction band minimum (for electrons) to place the carrier energies in our systems with respect to the redox potentials required for water splitting; this is depicted in Figure 5. The redox potentials of water at the extremes of pH are presented. We find that under acidic conditions, only C_2N and $C_{2-x}Ge_xN$ are capable of reducing hydrogen, while most materials have a VBM capable of oxidizing water for oxygen evolution. In extreme basic conditions, many of the systems have suitable band edge positions for both reactions, with the exception of *tg*-$C_{3-x}Si_xN_4$ (very shallow VBM) and C_2N, $C_{2-x}Si_xN$, and $C_{2-x}Ge_xN$ (very deep CBMs). The trends show another powerful demonstration that a mixture of the structural and compositional engineering provides a powerful tool for tuning the absolute band edge positions as well as the band gap.[74]

Figure 6 shows how changing the parent structure can affect the region of optical absorption of these materials. The C_2N parent structure shows the strongest optical absorption in the visible light region of the electromagnetic spectrum. Doping with Si and Ge results in lower absorption onsets, commensurate with reduced bandgaps; although the strength of absorption is slightly diminished upon doping, this should be considered when fully assessing the application of doping to improve performance. The *tg*-C_3N_4 structure has a lower optical absorption of visible light, but again, doping with Si leads to increased absorption in the visible range. Likewise, hg-C_3N_4 has a weaker absorption of visible light than C_2N. In *hg*-C_3N_4, the effect of doping is particularly pronounced, with Si doping leading to a much earlier optical absorption onset and strong activity in the visible range, demonstrating the importance of composition as well as structure for the realization of photocatalytic carbon nitride based monolayer materials.

4. CONCLUSIONS

Extensive HSE and PBE DFT simulations were carried out to engineer band structure properties of newly fabricated 2D carbon nitrides including *tg*-C_3N_4, *hg*-C_3N_4, C_2N, and C_3N by N-type, P-type, and isoelectronic doping agents such as B, N, P,

DOI: 10.1021/acsami.8b01729
ACS Appl. Mater. Interfaces 2018, 10, 11143−11151

Si, and Ge for the water splitting technique. We used structural stability, total and projected electronic density of states, absorbance spectra, and band edge alignment analyses to probe the carbon nitride structures.

While pristine and doped C_3N crystals contain zero or small band gaps (less than 1.23 eV), a fact which is not suitable for photocatalytic water splitting, bare *tg*-C_3N_4, *hg*-C_3N_4, and C_2N structures and the ones doped by isoelectronic Si and Ge agents show proper semiconducting properties. Specifically tuning the band structures with isoelectronic agents highly improves the band edge positions and visible absorbance spectra of the newly fabricated 2D carbon nitride structures.

This study shows that our doping technique can be applied to tune the bandgap of 2D carbon nitride nanostructures for photocatalytic water splitting, and we plan to study the effect of various band engineering methods such as structural aggregation and functionalization. We hope our study will shed light on developing and designing new photocatalytic low-dimensional materials to harvest hydrogen from water by the green solar water splitting approach and making the renewable method more feasible to both meet the growing energy needs and to reduce greenhouse gas emissions.

■ ASSOCIATED CONTENT

Supporting Information

The Supporting Information is available free of charge on the ACS Publications website at DOI: 10.1021/acsami.8b01729.

Two figures illustrating the metallic doped carbon nitride structures and the projected density of states (PDOS) of metallic doped carbon nitrides, and two tables listing the bond distances of pristine and doped carbon nitrides (PDF)

■ AUTHOR INFORMATION

Corresponding Author

*E-mail: chandraveer.singh@utoronto.ca.

ORCID

Meysam Makaremi: 0000-0003-3663-2045

Geoffrey A. Ozin: 0000-0002-6315-0925

Chandra Veer Singh: 0000-0002-6644-0178

Notes

The authors declare no competing financial interest.

■ ACKNOWLEDGMENTS

The authors gratefully acknowledge their financial support in parts by the Natural Sciences and Engineering Council of Canada (NSERC), University of Toronto, Connaught Global Challenge Award, and Hart Professorship. The computations were carried out through Compute Canada facilities, particularly SciNet and Calcul-Quebec. SciNet is funded by the Canada Foundation for Innovation, NSERC, the Government of Ontario, Fed Dev Ontario, and the University of Toronto, and we gratefully acknowledge the continued support of these supercomputing facilities.

■ REFERENCES

(1) Grätzel, M. Photoelectrochemical Cells. *Nature* **2001**, *414* (6861), 338−344.

(2) Chu, S.; Majumdar, A. Opportunities and Challenges for a Sustainable Energy Future. *Nature* **2012**, *488* (7411), 294−303.

(3) Lu, Q.; Yu, Y.; Ma, Q.; Chen, B.; Zhang, H. 2D Transition-Metal-Dichalcogenide-Nanosheet-Based Composites for Photocatalytic and Electrocatalytic Hydrogen Evolution Reactions. *Adv. Mater.* **2016**, *28* (10), 1917−1933.

(4) Yang, X.; Liu, R.; Lei, Y.; Li, P.; Wang, K.; Zheng, Z.; Wang, D. Dual Influence of Reduction Annealing on Diffused Hematite/FTO Junction for Enhanced Photoelectrochemical Water Oxidation. *ACS Appl. Mater. Interfaces* **2016**, *8* (25), 16476−16485.

(5) Katz, M. J.; Riha, S. C.; Jeong, N. C.; Martinson, A. B. F.; Farha, O. K.; Hupp, J. T. Toward Solar Fuels: Water Splitting with Sunlight And "rust" . *Coord. Chem. Rev.* **2012**, *256* (21−22), 2521−2529.

(6) Fujishima, A.; Honda, K. Electrochemical Photolysis of Water at a Semiconductor Electrode. *Nature* **1972**, *238* (5358), 37−38.

(7) Kamire, R. J.; Materna, K. L.; Hoffeditz, W. L.; Phelan, B. T.; Thomsen, J. M.; Farha, O. K.; Hupp, J. T.; Brudvig, G. W.; Wasielewski, M. R. Photodriven Oxidation of Surface-Bound Iridium-Based Molecular Water-Oxidation Catalysts on Perylene-3,4-Dicarboximide-Sensitized TiO2Electrodes Protected by an Al2O3Layer. *J. Phys. Chem. C* **2017**, *121* (7), 3752−3764.

(8) Zhou, Q.; Wu, M.; Zhang, M.; Xu, G.; Yao, B.; Li, C.; Shi, G. Graphene-Based Electrochemical Capacitors with Integrated High-Performance. Mater. *Today Energy* **2017**, *6*, 181−188.

(9) Li, Y.; Li, Y.-L.; Sa, B.; Ahuja, R. Review of Two-Dimensional Materials for Photocatalytic Water Splitting from a Theoretical Perspective. *Catal. Sci. Technol.* **2017**, *7* (3), 545−559.

(10) Yang, X.; Liu, R.; Du, C.; Dai, P.; Zheng, Z.; Wang, D. Improving Hematite-Based Photoelectrochemical Water Splitting with Ultrathin TiO2 by Atomic Layer Deposition. *ACS Appl. Mater. Interfaces* **2014**, *6* (15), 12005−12011.

(11) Tang, Q.; Zhou, Z. Graphene-Analogous Low-Dimensional Materials. *Prog. Mater. Sci.* **2013**, *58* (8), 1244−1315.

(12) Liu, X.; Guo, Q.; Qiu, J. Emerging Low-Dimensional Materials for Nonlinear Optics and Ultrafast Photonics. *Adv. Mater.* **2017**, *29* (14), 1605886.

(13) Novoselov, K. S.; Geim, A. K.; Morozov, S. V.; Jiang, D.; Zhang, Y.; Dubonos, S. V.; Grigorieva, I. V.; Firsov, A. A. Electric Field Effect in Atomically Thin Carbon Films. *Science* **2004**, *306* (5696), 666−669.

(14) Zhu, Y.; Murali, S.; Cai, W.; Li, X.; Suk, J. W.; Potts, J. R.; Ruoff, R. S. Graphene and Graphene Oxide: Synthesis, Properties, and Applications. *Adv. Mater.* **2010**, *22* (35), 3906−3924.

(15) Castro Neto, A. H.; Guinea, F.; Peres, N. M. R.; Novoselov, K. S.; Geim, A. K. The Electronic Properties of Graphene. *Rev. Mod. Phys.* **2009**, *81* (1), 109−162.

(16) Allen, M. J.; Tung, V. C.; Kaner, R. B. Honeycomb Carbon: A Review of Graphene. *Chem. Rev.* **2010**, *110* (1), 132−145.

(17) Mas-Ballesté, R.; Gómez-Navarro, C.; Gómez-Herrero, J.; Zamora, F. 2D Materials: To Graphene and beyond. *Nanoscale* **2011**, *3* (1), 20−30.

(18) Gibney, E. 2D or Not 2D. *Nature* **2015**, *522* (7556), 274−276.

(19) Mortazavi, B.; Rabczuk, T. Multiscale Modeling of Heat Conduction in Graphene Laminates. *Carbon* **2015**, *85*, 1−7.

(20) Balendhran, S.; Walia, S.; Nili, H.; Sriram, S.; Bhaskaran, M. Elemental Analogues of Graphene: Silicene, Germanene, Stanene, and Phosphorene. *Small* **2015**, *11* (6), 640−652.

(21) Kuang, Z.; Chen, Y.; Lu, Y.; Liu, L.; Hu, S.; Wen, S.; Mao, Y.; Zhang, L. Fabrication of Highly Oriented Hexagonal Boron Nitride Nanosheet/elastomer Nanocomposites with High Thermal Conductivity. *Small* **2015**, *11* (14), 1655−1659.

(22) Golberg, D.; Bando, Y.; Huang, Y.; Terao, T.; Mitome, M.; Tang, C.; Zhi, C. Boron Nitride Nanotubes and Nanosheets. *ACS Nano* **2010**, *4* (6), 2979−2993.

(23) Gong, Y.; Zhou, M.; Andrews, L. Spectroscopic and Theoretical Studies of Transition Metal Oxides and Dioxygen Complexes. *Chem. Rev.* **2009**, *109* (12), 6765−6808.

(24) Zhu, S.; Li, J.; Deng, X.; He, C.; Liu, E.; He, F.; Shi, C.; Zhao, N. Ultrathin-Nanosheet-Induced Synthesis of 3D Transition Metal Oxides Networks for Lithium Ion Battery Anodes. *Adv. Funct. Mater.* **2017**, *27* (9), 1605017.

(25) Wang, Q. H.; Kalantar-Zadeh, K.; Kis, A.; Coleman, J. N.; Strano, M. S. Electronics and Optoelectronics of Two-Dimensional

DOI: 10.1021/acsami.8b01729
ACS Appl. Mater. Interfaces 2018, 10, 11143−11151

Transition Metal Dichalcogenides. *Nat. Nanotechnol.* **2012**, *7* (11), 699−712.
(26) Chhowalla, M.; Shin, H. S.; Eda, G.; Li, L.-J.; Loh, K. P.; Zhang, H. The Chemistry of Two-Dimensional Layered Transition Metal Dichalcogenide Nanosheets. *Nat. Chem.* **2013**, *5* (4), 263−275.
(27) Chia, X.; Eng, A. Y. S.; Ambrosi, A.; Tan, S. M.; Pumera, M. Electrochemistry of Nanostructured Layered Transition-Metal Dichalcogenides. *Chem. Rev.* **2015**, *115* (21), 11941−11966.
(28) Ghuman, K. K.; Yadav, S.; Singh, C. V. Adsorption and Dissociation of H2O on Monolayered MoS2 Edges: Energetics and Mechanism from Ab Initio Simulations. *J. Phys. Chem. C* **2015**, *119* (12), 6518−6529.
(29) Naguib, M.; Mochalin, V. N.; Barsoum, M. W.; Gogotsi, Y. 25th Anniversary Article: MXenes: A New Family of Two-Dimensional Materials. *Adv. Mater.* **2014**, *26* (7), 992−1005.
(30) Anasori, B.; Lukatskaya, M. R.; Gogotsi, Y. 2D Metal Carbides and Nitrides (MXenes) for Energy Storage. *Nature Reviews Materials* **2017**, *2* (2), 16098.
(31) Editorial: 2D Materials. *Nat. Photonics* **2016**, *10* (4), 201.10.1038/nphoton.2016.61
(32) Kim, H. G.; Lee, H.-B.-R. Atomic Layer Deposition on 2D Materials. *Chem. Mater.* **2017**, *29* (9), 3809−3826.
(33) Mannix, A. J.; Kiraly, B.; Hersam, M. C.; Guisinger, N. P. Synthesis and Chemistry of Elemental 2D Materials. *Nature Reviews Chemistry* **2017**, *1* (2), 0014.
(34) Shi, L.; Zhao, T. Recent Advances in Inorganic 2D Materials and Their Applications in Lithium and Sodium Batteries. *J. Mater. Chem. A* **2017**, *5* (8), 3735−3758.
(35) Thomas, A.; Fischer, A.; Goettmann, F.; Antonietti, M.; Müller, J.-O.; Schlögl, R.; Carlsson, J. M. Graphitic Carbon Nitride Materials: Variation of Structure and Morphology and Their Use as Metal-Free Catalysts. *J. Mater. Chem.* **2008**, *18* (41), 4893.
(36) Algara-Siller, G.; Severin, N.; Chong, S. Y.; Björkman, T.; Palgrave, R. G.; Laybourn, A.; Antonietti, M.; Khimyak, Y. Z.; Krasheninnikov, A. V.; Rabe, J. P.; Kaiser, U.; Cooper, A. I.; Thomas, A.; Bojdys, M. J. Triazine-Based Graphitic Carbon Nitride: A Two-Dimensional Semiconductor. *Angew. Chem., Int. Ed.* **2014**, *53* (29), 7450−7455.
(37) Mahmood, J.; Lee, E. K.; Jung, M.; Shin, D.; Jeon, I.-Y.; Jung, S.-M.; Choi, H.-J.; Seo, J.-M.; Bae, S.-Y.; Sohn, S.-D.; Park, N.; Oh, J. H.; Shin, H.-J.; Baek, J.-B. Nitrogenated Holey Two-Dimensional Structures. *Nat. Commun.* **2015**, *6*, 6486.
(38) Mahmood, J.; Lee, E. K.; Jung, M.; Shin, D.; Choi, H.-J.; Seo, J.-M.; Jung, S.-M.; Kim, D.; Li, F.; Lah, M. S.; Park, N.; Shin, H.-J.; Oh, J. H.; Baek, J.-B. Two-Dimensional Polyaniline (C3N) from Carbonized Organic Single Crystals in Solid State. *Proc. Natl. Acad. Sci. U. S. A.* **2016**, *113* (27), 7414−7419.
(39) Lee, S. U.; Belosludov, R. V.; Mizuseki, H.; Kawazoe, Y. Designing Nanogadgetry for Nanoelectronic Devices with Nitrogen-Doped Capped Carbon Nanotubes. *Small* **2009**, *5* (15), 1769−1775.
(40) Li, J.; Cui, W.; Sun, Y.; Chu, Y.; Cen, W.; Dong, F. Directional Electrons Delivery via Vertical Channel between G-C3N4 Layers Promoting the Photocatalysis Efficiency. *J. Mater. Chem. A* **2017**, *5*, 9358−9364.
(41) Cui, W.; Li, J.; Cen, W.; Sun, Y.; Lee, S. C.; Dong, F. Steering the Interlayer Energy Barrier and Charge Flow via Bioriented Transportation Channels in G-C3N4: Enhanced Photocatalysis and Reaction Mechanism. *J. Catal.* **2017**, *352*, 351−360.
(42) Martha, S.; Nashim, A.; Parida, K. M. Facile Synthesis of Highly Active G-C3N4 for Efficient Hydrogen Production under Visible Light. *J. Mater. Chem. A* **2013**, *1* (26), 7816.
(43) Dong, M. M.; He, C.; Zhang, W. X. A Tunable and Sizable Bandgap of a G-C3N4/graphene/g-C3N4 Sandwich Heterostructure: A van Der Waals Density Functional Study. *J. Mater. Chem. C* **2017**, *5* (15), 3830−3837.
(44) Mortazavi, B.; Cuniberti, G.; Rabczuk, T. Mechanical Properties and Thermal Conductivity of Graphitic Carbon Nitride: A Molecular Dynamics Study. *Comput. Mater. Sci.* **2015**, *99*, 285−289.
(45) Mortazavi, B.; Rahaman, O.; Rabczuk, T.; Pereira, L. F. C. Thermal Conductivity and Mechanical Properties of Nitrogenated Holey Graphene. *Carbon* **2016**, *106*, 1−8.
(46) Yang, S.; Li, W.; Ye, C.; Wang, G.; Tian, H.; Zhu, C.; He, P.; Ding, G.; Xie, X.; Liu, Y.; Lifshitz, Y.; Lee, S. T.; Kang, Z.; Jiang, M. C3N—A 2D Crystalline, Hole-Free, Tunable-Narrow-Bandgap Semiconductor with Ferromagnetic Properties. *Adv. Mater.* **2017**, *29* (16), 1605625.
(47) Mortazavi, B. Ultra High Stiffness and Thermal Conductivity of Graphene like C3N. *Carbon* **2017**, *118*, 25−34.
(48) Makaremi, M.; Mortazavi, B.; Singh, C. V. Adsorption of Metallic, Metalloidic, and Nonmetallic Adatoms on Two-Dimensional C3N. *J. Phys. Chem. C* **2017**, *121* (34), 18575−18583.
(49) Du, J.; Xia, C.; Wang, T.; Xiong, W.; Li, J. Modulation of the Band Structures and Optical Properties of Holey C_2N Nanosheets by Alloying with Group IV and V Elements. *J. Mater. Chem. C* **2016**, *4* (39), 9294−9302.
(50) Ashwin Kishore, M. R.; Ravindran, P. Tailoring the Electronic Band Gap and Band Edge Positions in the C_2N Monolayer by P and As Substitution for Photocatalytic Water Splitting. *J. Phys. Chem. C* **2017**, *121* (40), 22216−22224.
(51) Ma, X. G.; Lv, Y. H.; Xu, J.; Liu, Y. F.; Zhang, R. Q.; Zhu, Y. F. A Strategy of Enhancing the Photoactivity of G-C3N4 via Doping of Nonmetal Elements: A First-Principles Study. *J. Phys. Chem. C* **2012**, *116* (44), 23485−23493.
(52) Kishore, M. R. A.; Ravindran, P. Enhanced Photocatalytic Water Splitting in a C2N Monolayer by C-Site Isoelectronic Substitution. *ChemPhysChem* **2017**, *18* (12), 1526−1532.
(53) Perdew, J. P.; Burke, K.; Ernzerhof, M. Generalized Gradient Approximation Made Simple. *Phys. Rev. Lett.* **1996**, *77* (18), 3865−3868.
(54) Vydrov, O. A.; Scuseria, G. E. Assessment of a Long-Range Corrected Hybrid Functional. *J. Chem. Phys.* **2006**, *125* (23), 234109.
(55) Kresse, G.; Furthmüller, J. Efficient Iterative Schemes for Ab Initio Total-Energy Calculations Using a Plane-Wave Basis Set. *Phys. Rev. B: Condens. Matter Mater. Phys.* **1996**, *54* (16), 11169−11186.
(56) Kresse, G.; Joubert, D. From Ultrasoft Pseudopotentials to the Projector Augmented - Wave Method. *Phys. Rev. B: Condens. Matter Mater. Phys.* **1999**, *59*, 1758.
(57) Grimme, S. Semiempirical GGA-Type Density Functional Constructed with a Long-Range Dispersion Correction. *J. Comput. Chem.* **2006**, *27* (15), 1787−1799.
(58) Gajdoš, M.; Hummer, K.; Kresse, G.; Furthmüller, J.; Bechstedt, F. Linear Optical Properties in the Projector-Augmented Wave Methodology. *Phys. Rev. B: Condens. Matter Mater. Phys.* **2006**, *73* (4), 045112.
(59) Zhang, R.; Li, B.; Yang, J. Effects of Stacking Order, Layer Number and External Electric Field on Electronic Structures of Few-Layer C_2N-h2D. *Nanoscale* **2015**, *7* (33), 14062−14070.
(60) Zhou, X.; Feng, W.; Guan, S.; Fu, B.; Su, W.; Yao, Y. Computational Characterization of Monolayer C3N: A Two-Dimensional Nitrogen-Graphene Crystal. *J. Mater. Res.* **2017**, *32* (15), 2993−3001.
(61) Xu, Y.; Gao, S. P. Band Gap of C3N4 in the GW Approximation. *Int. J. Hydrogen Energy* **2012**, *37* (15), 11072−11080.
(62) Silvi, B.; Savin, A. Classification of Chemical-Bonds Based on Topological Analysis of Electron Localization Functions. *Nature* **1994**, *371* (6499), 683−686.
(63) Mortazavi, B.; Makaremi, M.; Shahrokhi, M.; Raeisi, M.; Singh, C. V.; Rabczuk, T.; Pereira, L. F. C. Borophene Hydride: A Stiff 2D Material with High Thermal Conductivity and Attractive Optical and Electronic Properties. *Nanoscale* **2018**, *10*, 3759−3768.
(64) Cao, S.; Yu, J. G-C3N4-Based Photocatalysts for Hydrogen Generation. *J. Phys. Chem. Lett.* **2014**, *5* (12), 2101−2107.
(65) Liu, J. Effect of Phosphorus Doping on Electronic Structure and Photocatalytic Performance of G-C3N4: Insights from Hybrid Density Functional Calculation. *J. Alloys Compd.* **2016**, *672*, 271−276.

DOI: 10.1021/acsami.8b01729
ACS Appl. Mater. Interfaces 2018, 10, 11143−11151

(66) Power, P. P. π-Bonding and the Lone Pair Effect in Multiple Bonds between Heavier Main Group Elements. *Chem. Rev.* **1999**, *99* (12), 3463−3504.
(67) Demkov, A. A.; Sankey, O. F. Theoretical Investigation of Random Si-C Alloys. *Phys. Rev. B: Condens. Matter Mater. Phys.* **1993**, *48* (4), 2207−2214.
(68) Berding, M. A.; Sher, A.; van Schilfgaarde, M. Group-IV Semiconductor Compounds. *Phys. Rev. B: Condens. Matter Mater. Phys.* **1997**, *56* (7), 3885−3891.
(69) Demkov, A. A.; Sankey, O. F. Theoretical Investigation of Random Si-C Alloys. *Phys. Rev. B: Condens. Matter Mater. Phys.* **1993**, *48* (18), 2207−2214.
(70) Melissen, S.; Le Bahers, T.; Steinmann, S. N.; Sautet, P. Relationship between Carbon Nitride Structure and Exciton Binding Energies: A DFT Perspective. *J. Phys. Chem. C* **2015**, *119* (45), 25188−25196.
(71) Tachibana, Y.; Vayssieres, L.; Durrant, J. R. Artificial Photosynthesis for Solar Water-Splitting. *Nat. Photonics* **2012**, *6* (8), 511−518.
(72) Lewis, N. S.; Nocera, D. G. Powering the Planet: Chemical Challenges in Solar Energy Utilization. *Proc. Natl. Acad. Sci. U. S. A.* **2006**, *103* (43), 15729−15735.
(73) Kumagai, Y.; Butler, K. T.; Walsh, A.; Oba, F. Theory of Ionization Potentials of Nonmetallic Solids. *Phys. Rev. B: Condens. Matter Mater. Phys.* **2017**, *95* (12), 125309.
(74) Davies, D.; Butler, K.; Skelton, J. M.; Xie, C.; Oganov, A. R.; Walsh, A. Computer-Aided Design of Metal Chalcohalide Semiconductors: From Chemical Composition to Crystal Structure. *Chem. Sci.* **2018**, *9* (4), 1022.

DOI: 10.1021/acsami.8b01729
ACS Appl. Mater. Interfaces 2018, 10, 11143−11151